



NUMERICAL ANALYSES OF A PILED RAFT FOUNDATION WITH GRID-FORM DMWs UNDER LARGE EARTHQUAKE LOAD

Y. Shigeno⁽¹⁾, K. Yamashita⁽²⁾, J. Hamada⁽³⁾, N. Nakamura⁽⁴⁾

⁽¹⁾ Chief Researcher, Takenaka Research & Development Institute, shigeno.yoshimasa@takenaka.co.jp

⁽²⁾ Executive Manager, Takenaka Research & Development Institute, yamashita.kiyoshi@takenaka.co.jp

⁽³⁾ Chief Researcher, Takenaka Research & Development Institute, hamada.junji@takenaka.co.jp

⁽⁴⁾ Professor, Department of Architecture, Hiroshima University, naohiro3@hiroshima-u.ac.jp

Abstract

The seismic performance of a piled raft foundation with grid-form cement deep mixing walls (DMWs) under a large earthquake load is evaluated numerically. A base-isolated building located in Tokyo is modeled as a detailed three-dimensional finite element ground–structure interaction model. An elasto–plastic multi-surface model directly using the G- γ and h- γ characteristics as the input parameters is used for the soil, and a nonlinear model with tensile and shear criteria is applied to the stabilized soil. In this study, the model is first validated by comparing it with the observation records from the 2011 off the Pacific Coast of Tohoku Earthquake which was categorized as a medium earthquake at this site. And then a seismic response analysis using a large earthquake that is officially notified in Japanese design codes is conducted. According to the analysis, the maximum bending moment of the piles in the case with the grid-form DMWs is within the allowable criterion of the NM relation of the steel pipe–concrete composite pile, while that in the case without DMWs is markedly large and beyond the ultimate criterion. Consequently, it is found that the grid-form DMWs are very effective at reducing the sectional force of the piles to an acceptable level, even if the induced stress in the DMWs partially reaches its tensile strength during a large earthquake.

Keywords: piled raft, deep mixing walls, base-isolated building, 3D nonlinear FEM, seismic response analysis

1. Introduction

In recent years, piled raft foundations have been used in many countries as building foundations. The effectiveness of piled rafts at reducing average and differential settlements has been confirmed on soft clay and even on liquefiable sand with grid-form cement deep mixing walls (DMWs) [1, 2, 3]. The grid-form DMWs work as a countermeasure of liquefaction to increase the resistance of unstabilized soil and also to share the horizontal load. However, adding the grid-form DMWs as a new component of the foundation, the seismic behavior becomes more complicated and the necessity for detailed evaluation increases.

Field monitoring has been performed on a piled raft foundation with grid-form DMWs in soft ground supporting a 12-story building. The seismic response of the soil–foundation system was successfully recorded at the time of the 2011 off the Pacific Coast of Tohoku Earthquake [2]. In previous studies, seismic response analysis using a detailed three-dimensional (3D) finite element (FE) model was conducted for observation records [4, 5]. In the analyses, the soil was modeled with equivalent linear moduli since the recorded ground motion was categorized as a medium earthquake at this site. The analytical results agreed well with the observation records. However, the seismic performance during a large earthquake still needs to be evaluated.

The aim of this study is to evaluate the seismic performance of a piled raft foundation with grid-form DMWs under a large earthquake load. First, a numerical simulation applying a nonlinear soil model is conducted for data based on the 2011 off the Pacific Coast of Tohoku Earthquake. The accuracy of the model is evaluated in comparison with the observation records. Then, analysis is conducted for a large earthquake. In the evaluation, a nonlinear model with both tensile and shear criteria is applied for the stabilized soil.

2. Building, ground soil conditions, and foundation design

Fig. 1 shows a schematic view of the building and its foundation with the soil profile [2]. The building analyzed is a 12-story residential building located in Tokyo. The height is 38.7 m above the ground, and the cross section of the first floor is 33.25 m by 30.05 m. The building is a reinforced-concrete structure with a seismic base-isolation system; it was completed in 2008.

The soil down to a depth of 44 m is alluvial stratum. The upper 7 m is fill, soft silt and loose silty sand. The rest is very soft to medium silty clay. The stratum deeper than 44 m is diluvial sand and a gravel layer with SPT N-value of 60 or higher. The building is supported by a piled raft with grid-form DMWs which were employed to prevent liquefaction of the silty sand from GL -3 m to -7 m as well as to improve the bearing capacity of the raft foundation. The spacing between the DMWs is about 6 to 9 m, and the area replacement ratio is 25%. The locations of the seismic monitoring devices are also shown in Fig. 2.

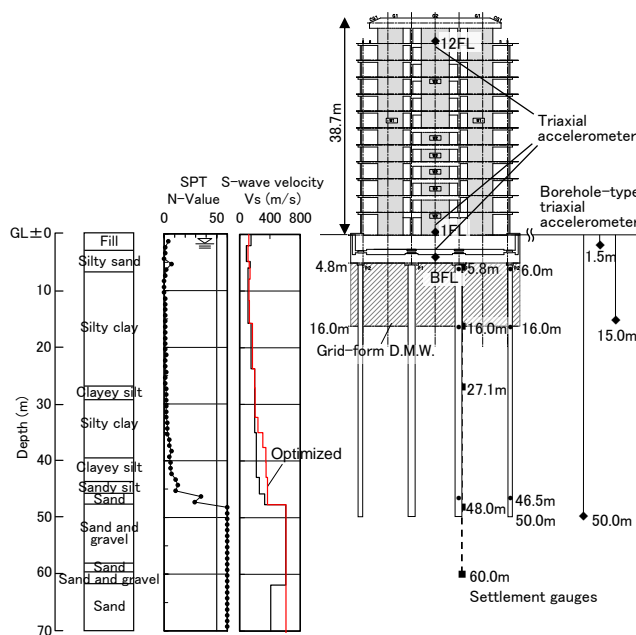


Fig. 1 - Schematic view of building foundation with soil profile

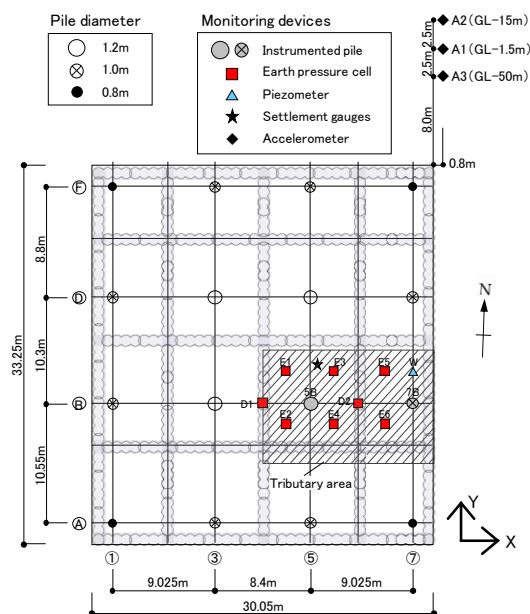


Fig. 2 - Foundation plan with locations of monitoring devices

3. Numerical analysis

3.1 Finite element mesh and program

Fig. 3 shows the finite element (FE) mesh, which has 213,622 elements and 656,543 degrees of freedom. The superstructure is modeled using elastic bars and shells, and the piles are modeled using elastic bars. Table 1 shows the material properties of the piles. The raft is modeled using elastic solid elements with the modulus of concrete. Rayleigh damping is applied to these components at a damping ratio of 2%. Fig. 4 shows a top view of the FE mesh beneath the raft. To consider the shape and volume of the piles, cavities in the shape of the piles are made in the model. The nodes of the piles and the adjacent ground nodes at the same depth are bound by rigid bar elements. The base isolation system is modeled using a tri-linear spring. The lateral boundaries are periodic boundaries, and are positioned 60 m outside of the building to minimize the boundary effect. The bottom is a viscous boundary at a depth of 75 m from the ground surface. The software is an in-house program called MuDIAN [6]. It is parallelized using the hybrid parallel method and is able to analyze a large-DOF model at high speed [7].

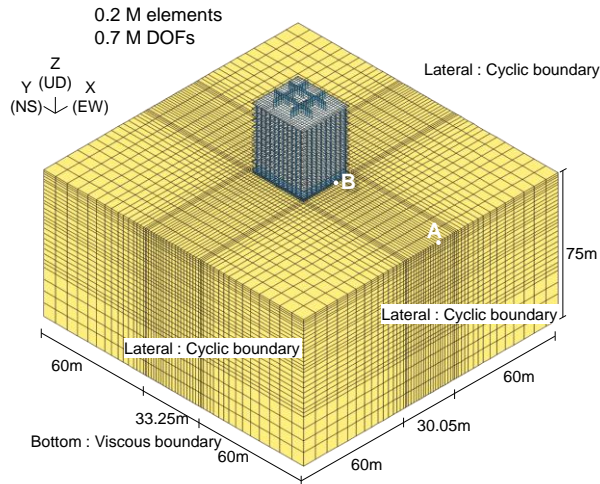


Fig. 3 - FE mesh of ground–structure interaction model

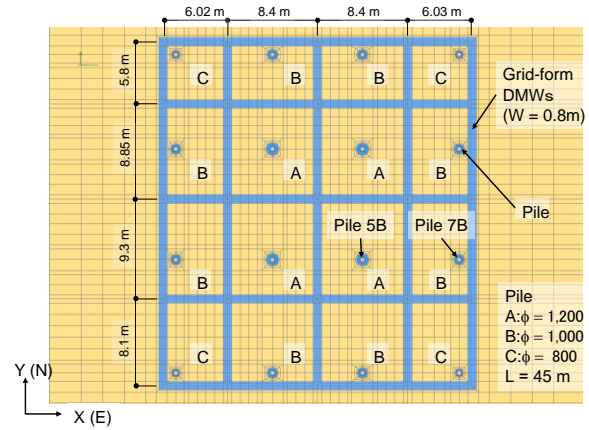


Fig. 4 - Magnified top view of FE mesh under raft

Table 1 - Material characteristics of piles

Pile diameter (mm)	Young's modulus (MN/m ²)	A _e of SC pile (m ²)	I _e of SC pile (m ⁴)	A _e of PHC pile (m ²)	I _e of PHC pile (m ⁴)
800	40000	0.3268	0.02199	0.2441	0.01455
1000	40000	0.4649	0.04899	0.3633	0.03437
1200	40000	0.6714	0.07114	0.5054	0.06958

A_e : Equivalent cross-sectional area
I_e : Equivalent area moment of inertia

3.2 Constitutive model of soil

A multi-hardening model proposed by Shiomi and Fujiwara [8] is used as the constitutive model for the soil. This model is based on the multi-dimensional Ishihara–Yoshida model [9, 10]. The Ishihara–Yoshida model is a multi-surface model and is characterized using $G-\gamma$ and $h-\gamma$ characteristics directly as input data. This model uses a non-linear elastic stress–strain relation. This often causes overestimation of the strain under multi-directional input. A multi-hardening model uses Mohr–Coulomb model for the stress–strain relation. Therefore the direction of softening can be considered.

The nonlinearity within the yield surface is expressed by a hardening coefficient H' defined by equation (1). G_T is the tangential shear modulus evaluated from the $\tau-\gamma$ curve obtained from the $G-\gamma$ characteristics.

$$H' = \frac{G_T}{1 - G_T/G_0} \quad (1)$$

The hardening coefficient H' appears in the denominator of the plastic multiplier $d\lambda$ expressed by an elastic modulus tensor \mathbf{D}_e and a yield function f as follows.

$$d\lambda = \frac{\frac{\partial f}{\partial \boldsymbol{\sigma}}^T \mathbf{D}_e d\boldsymbol{\varepsilon}}{H' + \frac{\partial f}{\partial \boldsymbol{\sigma}}^T \mathbf{D}_e \frac{\partial f}{\partial \boldsymbol{\sigma}}} \quad (2)$$

3.3 Soil properties

The shear wave velocity profile of the ground is obtained using an optimization method [4]. The error in the transfer function is used as a cost function. The observation records of small earthquakes that occurred before the 2011 off the Pacific Coast of Tohoku Earthquake were used as the target data. The initial V_S is the P-S logging result, and the optimized V_S distribution is shown in Fig. 1 with the logged V_S . The nonlinear characteristics of the ground were obtained from tests of in-situ samples and they are shown in Fig. 5. In this analysis, liquefaction is not considered though it may occur in the sand layer between depths of 3 and 7 m under large earthquakes. Further research is necessary to examine the effect of liquefaction.

3.4 Constitutive model of stabilized soil

The DMWs fail by tension or shear during earthquakes. The Mohr–Coulomb model is often applied to stabilized soil, but it generally gives a larger tensile strength than the real value. The tensile criterion has to be used for correct evaluation. The tensile criterion σ_t is expressed by the maximum principal stress σ_1 (note that tension is positive) and it is expressed by stress invariants J'_2 and σ_m by applying a Lode angle θ ($-\pi/6 < \theta < \pi/6$)

$$\sigma_t = \sigma_1 = \frac{2(J'_2)^{\frac{1}{2}}}{\sqrt{3}} \sin\left(\theta + \frac{2\pi}{3}\right) + \sigma_m \quad (3)$$

where J'_2 is the second invariant of deviatoric stress, and σ_m is the mean stress. Also, the Mohr–Coulomb criterion for the shear failure is expressed using stress invariants as follows

$$\sigma_m \sin \phi + (J'_2)^{\frac{1}{2}} \left(\cos \theta - \frac{1}{\sqrt{3}} \sin \theta \sin \phi \right) = c \cos \phi \quad (4)$$

where ϕ is the friction angle and c is the cohesion. These criteria are shown in Fig. 6. The tensile strength is evaluated correctly by taking a lower strength between the two criteria.

The Hayashi–Hibino model [11] is used for the two-criterion model described here in this study. The Hayashi–Hibino model is a nonlinear elastic model, and the elastic modulus is reduced to the specified value at failure. This model is able to evaluate nonlinearity within the failure criteria. The proximity ratio to the criteria R defined in Fig. 6 is used. R takes the minimum value for the two criteria and becomes 0 when the stress reaches the criteria. The elastic moduli are reduced according to R in the following equations using the parameter a .

$$E = R^{\frac{1}{a}} E_0, \quad 0.45 - \nu = R^{\frac{1}{2a}} (0.45 - \nu_0) \quad (5)$$

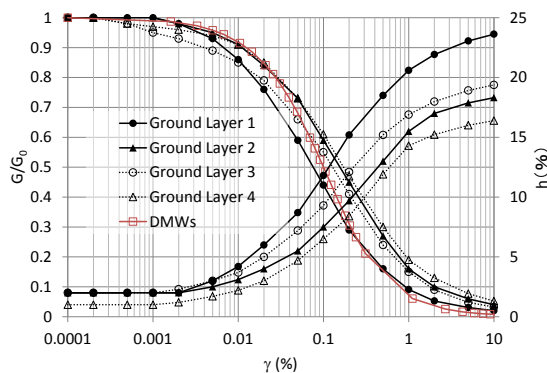


Fig. 5 - Strain dependence characteristics of ground and DMWs

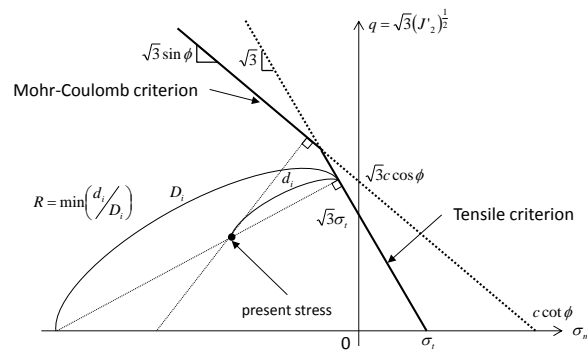


Fig. 6 - Criteria of the Hayashi–Hibino model

3.5 Properties of stabilized soil

The properties of the stabilized soil are determined from the in-situ unconfined compressive strength $q_0 = 3.8$ MPa that is the average value of 36 core samples aged 28 days with a covariance of 0.25 [12]. The tensile strength is set to $0.2q_0 = 0.76$ MPa, the cohesion is set to $0.3q_0 = 1.14$ MPa and the initial shear modulus is set to 1300 MPa. The friction angle is assumed to be 30 degrees. The initial vertical stress of the DMWs is 300 kPa, which is the measured contact pressure between the raft and the DMWs [2]. The horizontal stress is calculated by multiplying the pressure and the coefficient of earth pressure at rest. The parameter a of the Hayashi–Hibino model is determined as 1.0 by simulating the unconfined compression test. The G - γ characteristic of the DMWs is shown in Fig. 5. The shear modulus at failure is assumed to be one-thousandth of the initial value.

4. Analysis results

4.1 Seismic response analysis for the 2011 off the Pacific Coast of Tohoku Earthquake

The analysis using the cited nonlinear soil model is conducted under the input motion based on the records of the 2011 off the Pacific Coast of Tohoku Earthquake [13]. The same model is also used for the DMWs. Fig. 7 shows the input motion in each direction. These input motions are categorized as a medium earthquake considering the recorded maximum acceleration at the ground surface shown in Fig. 8. Fig. 8 shows the profiles of the peak acceleration and relative displacement to the point at GL -50 m of the center of the superstructure and the ground at the observation point shown in Fig. 2. The profiles are in the EW direction. The recorded peak ground acceleration at depth GL -1.5 m was 174.8 cm/s^2 . The results of the equivalent linear analysis are also shown as dotted lines. The results of the nonlinear analysis agree well with the observations just as in the equivalent linear analysis, especially the peak ground displacement. Fig. 9 shows the profiles of the peak bending moment of the piles. These results also agree well with the observations. From these results, the validity of the nonlinear analysis model for a middle-scale earthquake has been confirmed. Also, the stress in the DMWs was much less than the tensile strength.

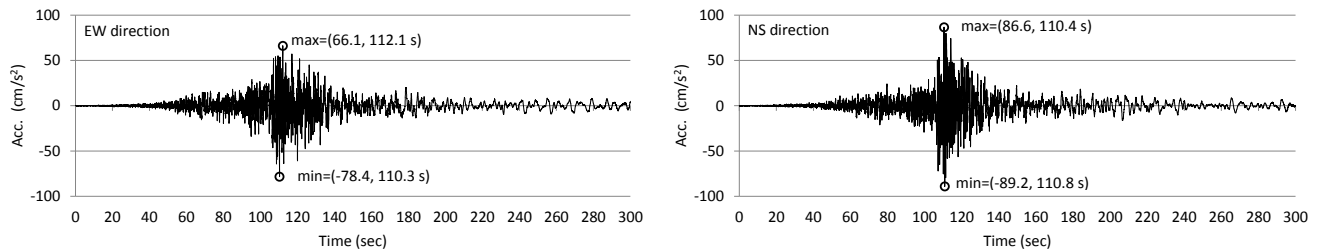


Fig. 7 - Input motion (2E) based on records of 2011 off the Pacific Coast of Tohoku Earthquake at GL -75 m

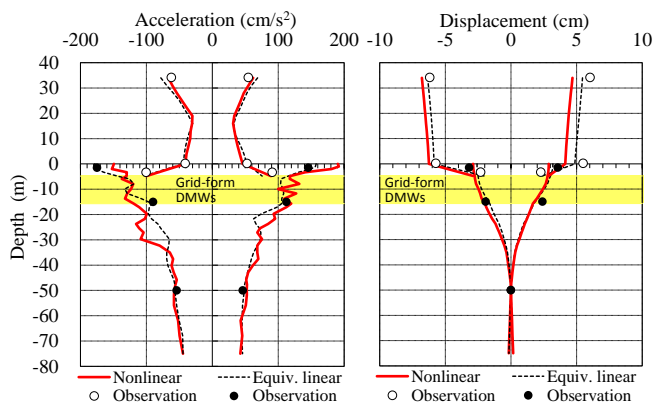


Fig. 8 - Peak response profiles of superstructure and ground (EW direction)

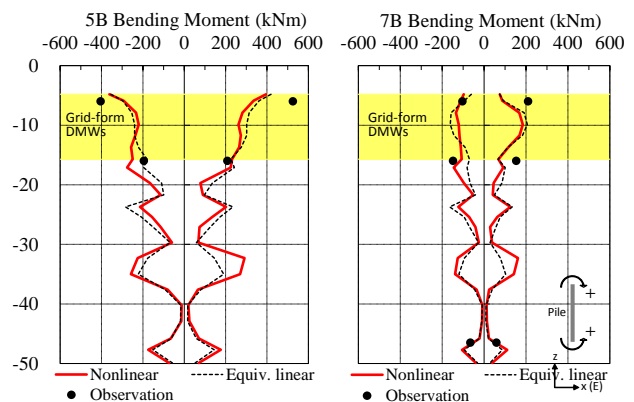


Fig. 9 - Profiles of peak bending moment of piles (EW direction)

4.2 Seismic response analysis under large earthquake load

4.2.1 Large earthquake

A large earthquake has been chosen from level 2 waves that are officially notified in Japanese design code. Level 2 waves are used for the performance design of a building. The recurrence interval of these waves is considered to be about 500 years. The waves are defined according to the officially notified acceleration response spectrum and generated using various phase data. In this paper, the level 2 wave generated using the Kobe phase data (referred as the Kobe phase herein after) is used. The Kobe phase is generated using the records from the Great Hanshin Earthquake (1995) that struck the Kobe Marine Observatory. Fig.10 shows the input motion in each direction. Fig. 11 shows the acceleration response spectrum of the wave, as well as the response spectra of the 2011 off the Pacific Coast of Tohoku Earthquake and the level 1 wave that is used for the allowable stress design.

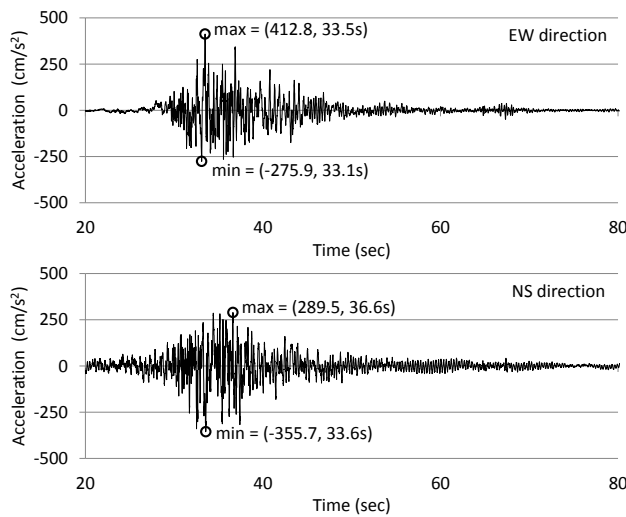


Fig. 10 - Level 2 Kobe phase waves (2E)

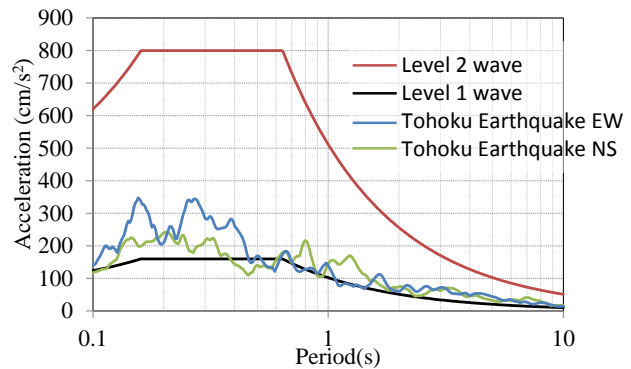


Fig. 11 - Acceleration response spectrum of level 2 wave, level 1 wave, and Tohoku Earthquake (GL -75 m)

4.2.2 Analytical results of Kobe phase

Two analysis cases were examined. One is with the DMWs whose properties are described in section 3.5, and the other is the case without DMWs.

Fig. 12 shows the acceleration response spectrum of the ground surface at the far field in the NS direction. The far field means that the response is derived from the analysis using the soil column model here. The spectra at the bottom of the raft in both cases (GL -4.8 m at point B in Fig. 3) are also shown in the figure. Comparing the response at the far field and the raft, the input loss due to the interaction is confirmed. The response of the raft in the case with DMWs is also smaller than that of the case without DMWs. This indicates that the existence of the grid-form DMWs causes a larger input loss. Fig. 13 shows the profiles of the peak acceleration at the center of the superstructure and the raft in the NS direction together with those of the ground at point B. The response of the soil column model is also shown as far field. The peak ground surface acceleration at the far field is 396 cm/s². In the case with DMWs, the peak responses are 262 cm/s² at the raft and 144 cm/s² on the first floor. The reduction rate by the base isolation system is 55%. In the case without DMWs, the peak responses are 330 cm/s² and 127 cm/s², and the reduction rate is 38%. Fig. 14 shows the profiles of the peak displacement at the center of the superstructure and the ground at point B. The displacement is relative to GL -49.9 m and in the NS direction. The peak responses at the bottom of the raft are -13.5 cm and 10.6 cm in the case with DMWs, which are smaller than -16.5 cm and 15.4 cm in the case without DMWs. In addition, those of the ground surface at the point A are similar between the two cases. The peak deformation is 18.7 cm in the case with DMWs and 18.8 cm in the case without DMWs. This indicates that the horizontal ground deformation beneath the raft is significantly reduced by the grid-form DMWs.

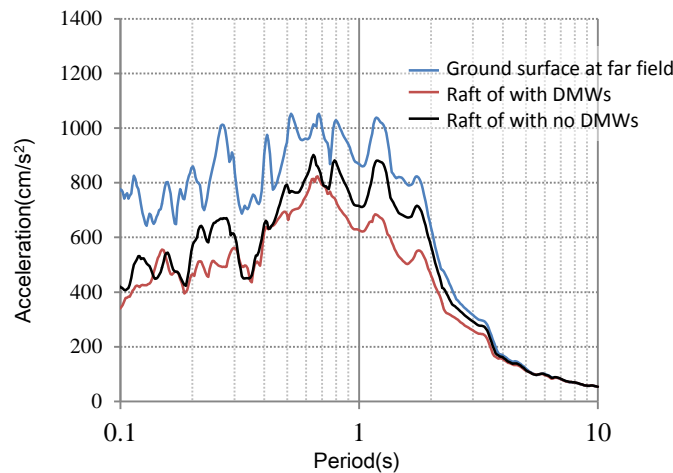


Fig. 12 - Acceleration response spectrum at ground surface at far field and raft (NS direction)

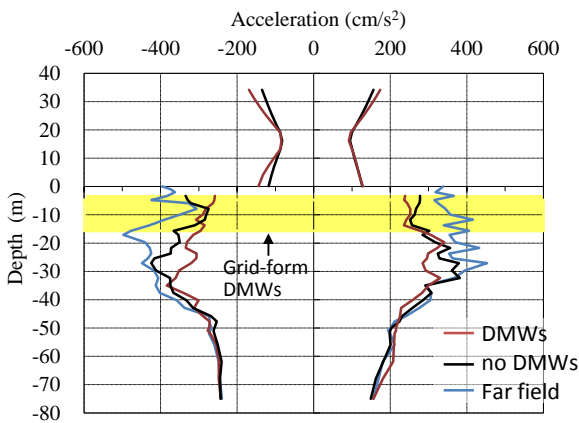


Fig. 13 - Peak acceleration profile of superstructure, ground at point B and far field (NS direction)

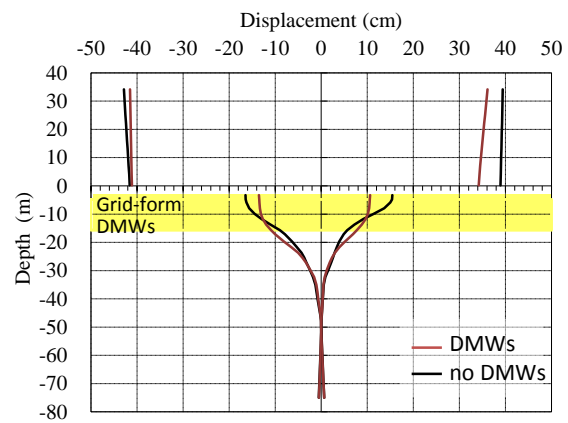
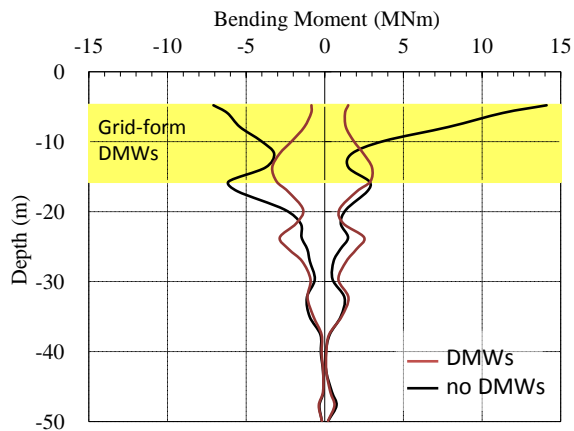
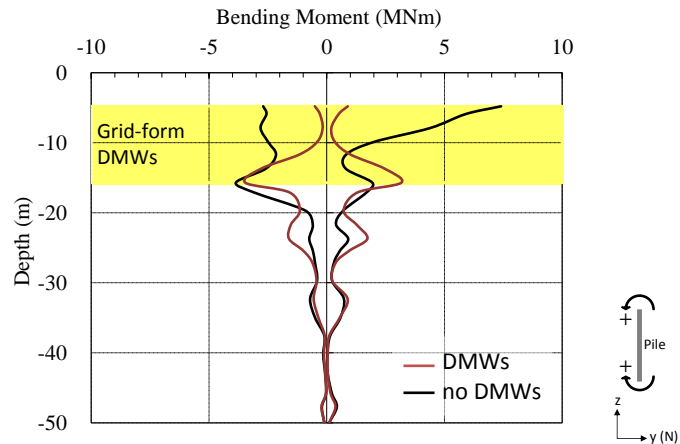


Fig. 14 - Peak displacement profiles relative to GL -49.9 m of superstructure and ground at point B (NS direction)

Fig. 15 shows the profiles of the peak bending moment in piles 5B and 7B in the NS direction. The peak value near the pile head in the case with DMWs is remarkably smaller than those in the case without DMWs. Also, the positive peak of the pile head is fairly larger than the negative peak in the case without DMWs. Fig. 16 shows the time history of the bending moment of the pile head of Pile 5B and the relative displacement of the top of the DMWs (GL -4.8 m) to the bottom of them (GL -15.7 m) at point B in the NS direction. The deformation in the case with DMWs is much smaller than in the case without DMWs. This also indicates that the deformation is decreased by the DMWs. In the case without DMWs, the first large positive deformation at 34.0 s may cause the strong soil nonlinearity and the residual deformation to occur. The bending moment corresponds to this and results in the peak asymmetry and the residual moment. However, in the case with DMWs, the deformation is much smaller, and a large peak asymmetry and residual moment do not occur in the bending moment. Fig. 17 shows the profiles of the displacement relative to GL -15.7 m at point B and the bending moment of 5B at 34.0 s and 35.0 s when the pile head specifies the peak moment in the case without DMWs. In the case with DMWs, the deformation of the soil enclosed by the DMWs is small and results in a small bending moment near the pile head. However, the moment at the bottom of the DMWs is large, as if this point is the pile head, and the grid-form DMWs and the surrounding soil move integrally. On the other hand, in the case without DMWs, the profiles show the general pile foundation pattern with the fixed pile head. The deformation near the pile head is large and causes the large bending moment.



(a) Pile 5B



(b) Pile 7B

Fig. 15 - Profiles of peak bending moment of piles 5B and 7B (NS direction)

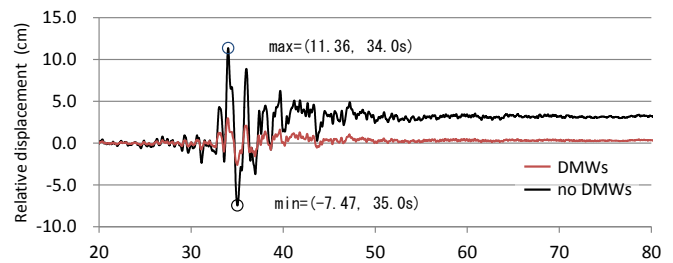
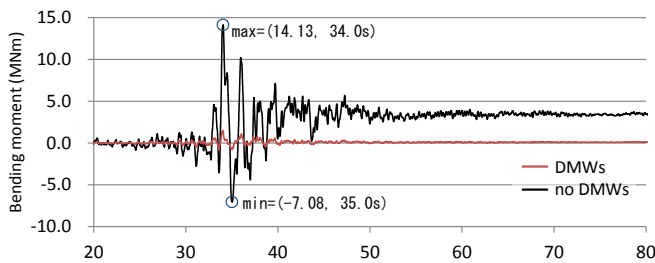
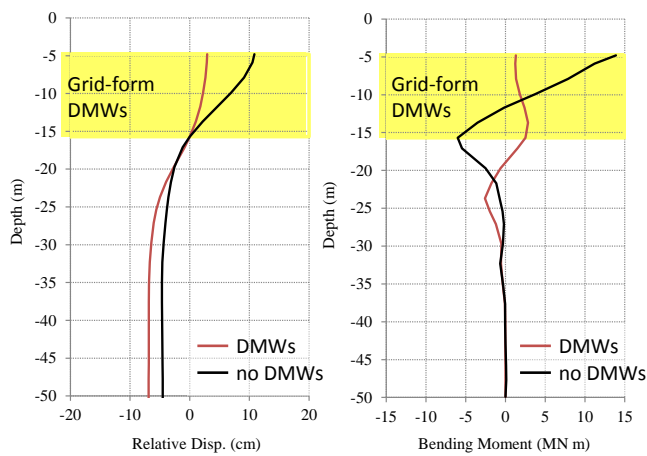
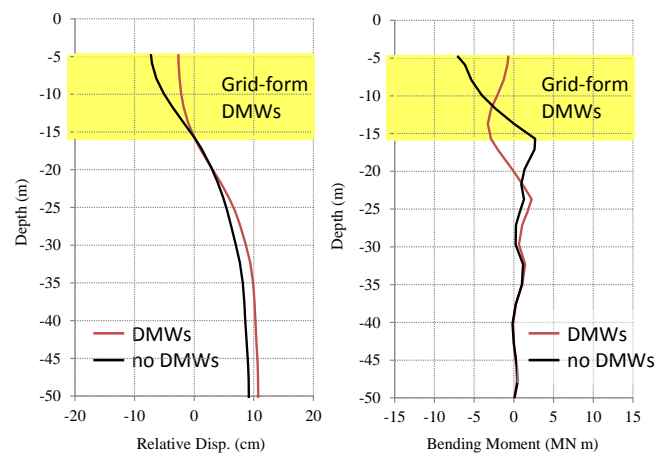


Fig. 16 - Time history of displacement of bottom of raft at B relative to GL -15.7 m and bending moment at pile head of 5B (NS direction)



(a) 34.0 s

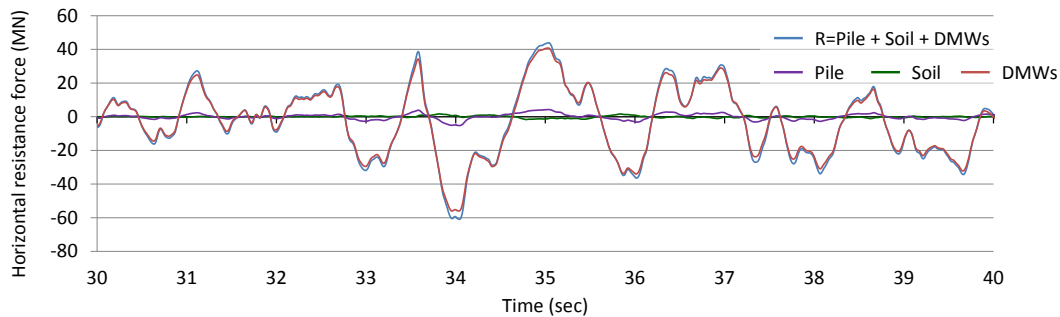


(b) 35.0 s

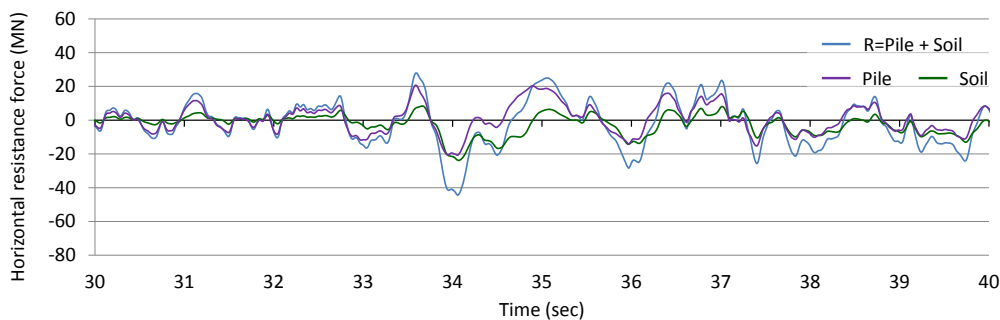
Fig. 17 - Profile of ground displacement at B relative to GL -15.7 m and bending moment of pile 5B

Fig 18 shows the time history of the horizontal resistance forces of the foundation acting on the raft. The resistance forces are shearing force at the pile heads, on the top of the grid-form DMWs and the soil enclosed by DMWs. Sum of these forces is also shown as blue line indexed R. They resist the horizontal driving forces, which are the inertial force from the superstructure and the raft, and passive force acting on the side of the buried raft. In the case with DMWs, a considerable amount of the horizontal force is carried by the grid-form DMWs. The DMWs share 91% of the total force, while the soil shares 8% and the piles share 1% at 34.0 s when the bending moment of the pile head specifies the largest value in both cases. On the other hand, the pile and the soil below the raft resist against the horizontal force almost evenly in the case with no DMWs. The piles share 54% and the soil share 46% at the same time. This is the reason for the remarkably smaller bending moment of the pile head in the case with DMWs. Moreover, the total horizontal force is larger in the case with DMWs. This is due to the strong horizontal resistance of the grid-form DMWs.

Fig. 19 shows the tensile and the shear failure zone in the grid-form DMWs. The tensile failure zone means that the maximum ratio of the maximum principal stress σ_1 to the tensile strength σ_t is larger than 0.95. The shear failure zone means the maximum ratio of the equivalent stress q to that at failure q_f is larger than 0.95. Both stresses are the mean values of eight Gauss points in each element. The tensile failure zone is mostly limited in the bottom part of the DMWs and the most part is sound. Fig. 20 shows the deformation of the grid-form DMWs with the specification of the failure zone at 35.0 s and 80.0 s. Time 35.0 s is when the bending moment of the pile head of 5B peaks on the negative side and time 80.0 s is when the motion almost settles. The figure indicates that the tensile failure occurs mainly in the bottom part due to the bending deformation, and at the time of 80.0 s, the deformation remains where the failure occurs. It is also shown that the top portion of the DMWs does not deform in such a direction that bending occurs. This is due to the constraint by the raft at the bottom of it and the soundness of the top portion is maintained. Moreover, shear failure is not almost seen in the DMWs as shown in Fig. 19(b).

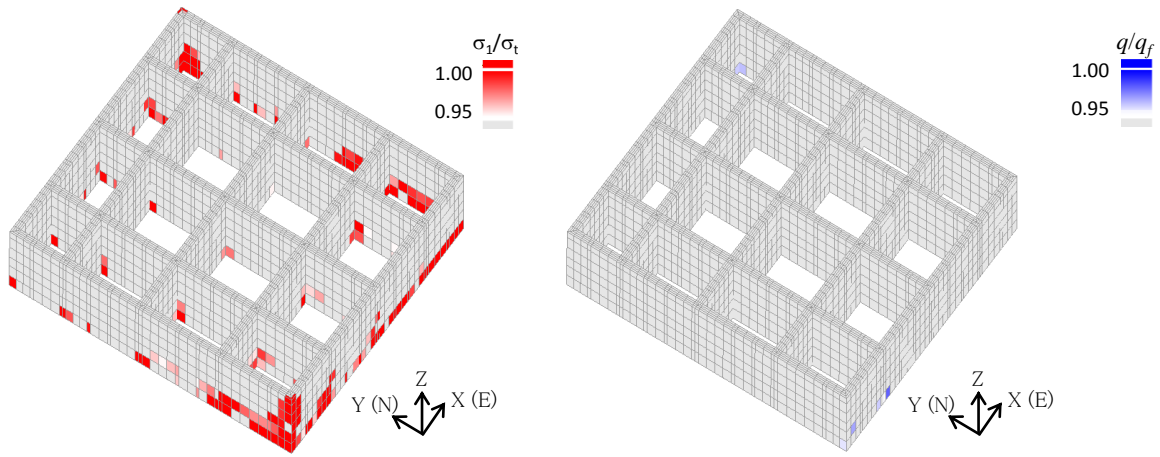


(a) Case with DMWs



(b) Case with no DMWs

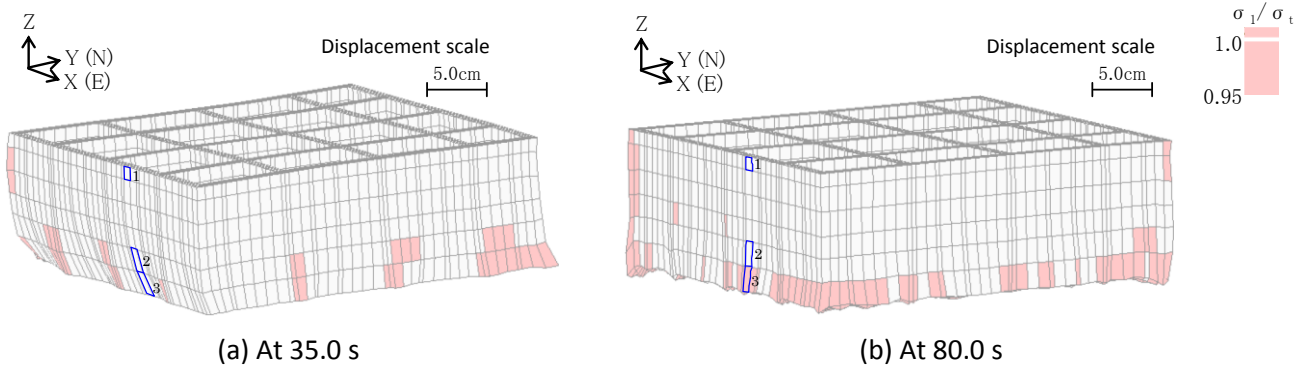
Fig. 18 - Time history of horizontal resistance force of foundation



(a) Tensile failure

(b) Shear failure

Fig. 19 - Tensile and shear failure zone in grid-form DMWs



(a) At 35.0 s

(b) At 80.0 s

Fig. 20 - Deformation and tensile failure zones of grid-form DMWs

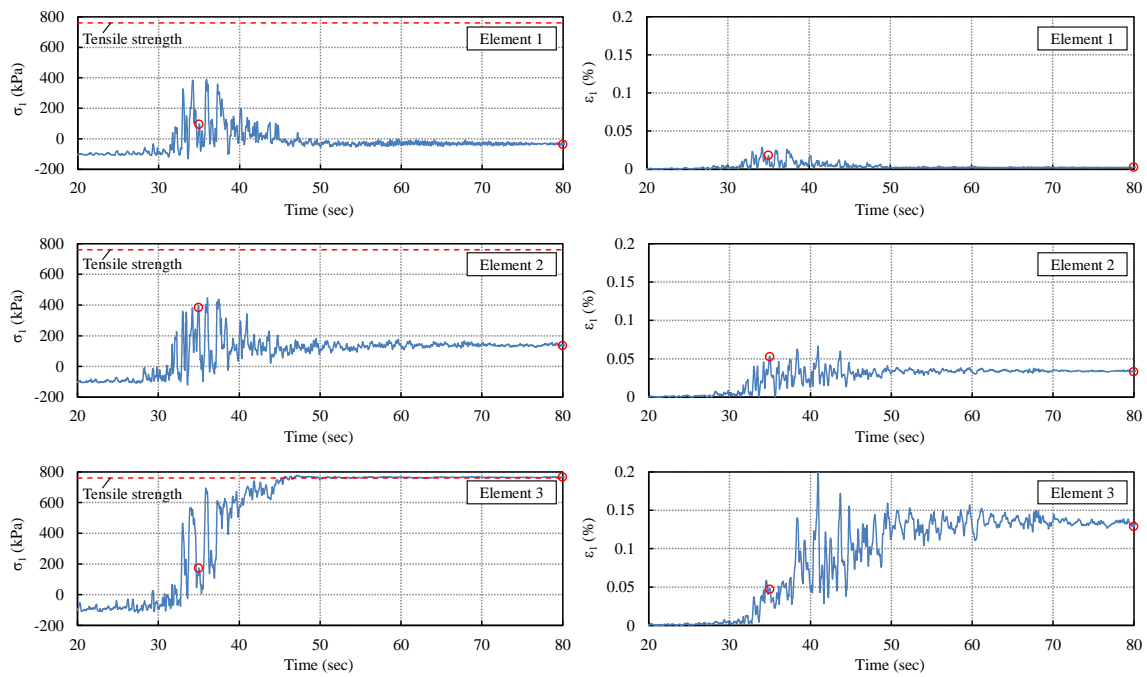


Fig. 21 - Time histories of the maximum principal stress and strain

Fig. 21 shows the time histories of the maximum principal stress σ_1 and strain ϵ_1 of the elements shown in Fig. 20. The red dotted line is the tensile strength $\sigma_t = 760$ kPa, and the red circles mark the time specified in Fig. 20. In element 1, which is near the head of the DMWs, the peak maximum principal stress is 388 kPa, which is about half of the tensile strength. Also, the induced tensile strain ϵ_1 is as small as 0.03% because the deformation of the DMWs near the head is small. In element 2, bending deformation occurs as specified in Fig. 20, but the peak value of σ_1 is the same level as element 1, and the stress does not reach the tensile strength. The principal tensile stress and strain remain after the main motion due to the residual bending deformation, as shown in Fig. 20(b). In element 3, the maximum principal stress reaches the tensile strength due to the bending deformation. Only the element located near the bottom of the DMWs fails among the selected elements. Also, the tensile strain is 0.23% at the peak and remains at about 0.15% after the main motion. Although softening may occur after the tensile failure, the constitutive model used here is unable to express it. Consideration of the softening after tensile failure is an issue to be addressed in the ongoing study.

Fig. 22 shows the relationship between the axial force and the bending moment of Piles 5B and 7B, together with the design interaction curves of the steel pipe–concrete composite (SC) pile which is used in the top portion at 12 m. Here, the axial force means the sum of the statically measured pile head load and the maximum and minimum dynamic incremental force in the analysis, and the bending moment means the maximum value along the SC pile which is obtained by combining the components in the NS and EW directions. The numerical results indicate that the maximum bending moments in the case with DMWs is below the allowable criterion (the unit stress at the edge of the concrete is in the elastic condition). In contrast, the maximum bending moments in the case without DMWs are clearly beyond the ultimate criterion (the unit stress at the edge of the concrete reaches the compressive strength). Hence, the grid-form DMWs are quite effective at reducing pile bending moments to an acceptable level, even if the induced stress in the stabilized soil partially reaches the tensile strength under the large earthquake load. Namikawa et al. [14] have pointed out that the grid-form DMWs can be designed more rationally using a performance-based design method in which a partial failure of the DMWs is accepted. The numerical results suggest that the present nonlinear 3D FE model can provide adequate solutions for the performance-based seismic design of piled rafts with grid-form DMWs.

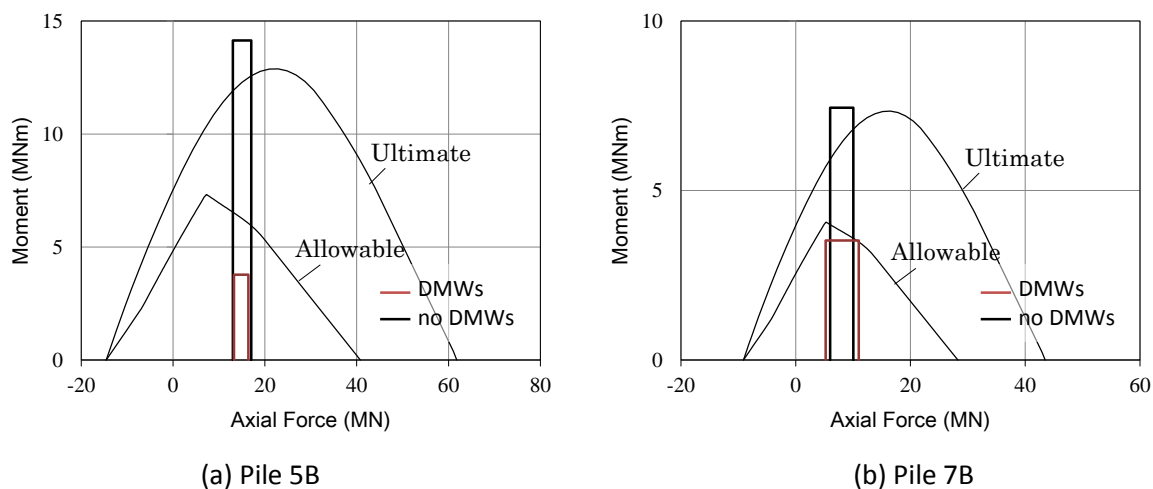


Fig. 22 - NM-relationship of SC piles, and calculated values

5. Conclusion

Seismic response analysis of a piled raft foundation with grid-form DMWs using a 3D nonlinear FE model under a large earthquake load was performed based on previous successful simulation analyses under a medium earthquake load. According to the results, the bending moments of piles around the pile head are markedly large in the case without DMWs and beyond the ultimate criterion of the NM relation of the SC pile. While those in



the case employing the grid-form DMWs are below the allowable criterion. Consequently, it is found that the grid-form DMWs are very effective at reducing the sectional force of piles to an acceptable level even if the induced stress in the DMWs partially reaches its tensile strength during a large earthquake. In other words, the sectional force of the piles is significantly affected by the tensile strength of the stabilized soil.

Acknowledgements

The results were obtained using the K computer at the RIKEN Advanced Institute for Computational Science (Proposal number hp150063) and the TSUBAME2.5 supercomputer at the Tokyo Institute of Technology supported by the MEXT Project for Creation of Research Platforms and Sharing of Advanced Research Infrastructure. This work was also supported by the JSPS KAKENHI Grant (No. 26289197).

References

- [1] Yamashita, K., Yamada, T. and Hamada, J. (2011): Investigation of settlement and load sharing on piled rafts by monitoring full -scale structures, *Soils & Foundations*, Vol. 51, No. 3, 513–532.
- [2] Yamashita, K., Hamada, J., Onimaru, S. and Higashino, M. (2012): Seismic behavior of piled raft with ground improvement supporting a base-isolated building on soft ground in Tokyo, *Soils & Foundations*, Vol. 52, No. 5, 1000–1015.
- [3] Yamashita, K., Hamada, J. and Tanikawa, T. (2016): Static and seismic performance of a friction piled combined with grid-form deep mixing walls in soft ground, *Soils & Foundations*, Vol. 56, No. 3 (to be published).
- [4] Onimaru, S., Hamada, J., Nakamura, N. and Yamashita, K. (2012): Dynamic soil-structure interaction of a building supported by piled raft and ground improvement during the 2011 Tohoku Earthquake, *Proc. of the 15thWCEE*, Lisbon, Portugal.
- [5] Hamada, J., Shigeno, Y., Onimaru, S., Tanikawa, T., Nakamura, N. and Yamashita, K. (2014): Numerical analysis on seismic response of piled raft foundation with ground improvement based on seismic observation records, *Proc. of the 14th IACMAG*, Kyoto, Japan.
- [6] Shiomi, T., Yoshizawa, M., Onimaru, S. and Tsukuni, S. (1998): Development of structural analysis system considering non-linear behaviors of soil and structure, *Takenaka Technical Research Report*, No.54, 1–8 (in Japanese).
- [7] Shigeno, Y., Hamada, J. and Nakamura, N. (2014): Hybrid parallelization of earthquake response analysis using K computer, *Proc. of the 14th IACMAG*, Kyoto, Japan.
- [8] Shiomi, T. and Fujiwara, Y. (2014): Liquefaction analysis of Urayasu-site by the multi-hardening model, *Proc. of the special symposium of JGS -Overcoming the Great East Japan Earthquake-*, 141–145 (in Japanese).
- [9] Ishihara, K., Yoshida, N. and Tsujino, S. (1985): Modeling of stress-strain relations of soils in cyclic loading, *Proc. of the 5th International Conference for Numerical Method in Geomechanics*, Nagoya, Japan, Vol. 1, 115–143.
- [10] Yoshida, N. and Tsujino, S. (1993): A simplified practical stress–strain model for the multi-dimensional analysis under repeated loading, *The 28th Japan national conference on soil mechanics and foundation engineering*, 1221–1224 (in Japanese).
- [11] Motojima, M., Hibino S. and Hayashi, M. (1978): Development of computer program for stability analysis of excavation, *Central Research Institute of Electric Power Industry Report No 377012* (in Japanese).
- [12] Yamashita, K., Tanikawa, T., Shigeno, Y. and Hamada, J. (2015): Vertical load sharing of piled raft with grid-form deep mixing walls, *Proc. of Conference on Deep Mixing 2015*, 437–446.
- [13] Shigeno, Y. (2015): Nonlinear analysis of seismic response of a base isolated building on a piled raft foundation with grid-form ground improvement, *Proc. of the 15th Asian Regional Conference on Soil Mechanics and Geotechnical Engineering*, Fukuoka, Japan.
- [14] Namikawa, T., Koseki, J. and Suzuki, Y. (2007): Finite element analysis of lattice-shaped ground improvement by cement-mixing for liquefaction mitigation, *Soils & Foundations*, Vol. 47, No.3, 559–576.